Water Practice & Technology

IWA PUBLISHING

Water Practice & Technology Vol 17 No 11, 2422 doi: 10.2166/wpt.2022.129

$KMnO_4$ modified biochar derived from swine manure for tetracycline removal

Zan Fu[a], Yurong Chen[a], Yanyan Lu[b], Yue Wang[a], Jiahui Chen[a], Youxin Zhao[a], Mengya Yang[a] and Xiaofei Tian[a,*]

[a] School of Geography and the Environment, Liaocheng University, Liao'cheng 252059, China
[b] Liaocheng University Dongchang College, Liao'cheng 252000, China
*Corresponding author. E-mail: tianxiaofei624@163.com

XT, 0000-0001-5973-6109

ABSTRACT

Tetracycline (TC) is widely used in the livestock industry, but undigested TC is excreted with livestock waste and accumulates in the environment. In this study, swine manure-derived biochar (SBC) was modified with $KMnO_4$ (MnOx-SBC), and used to remove TC. SEM-EDS, FTIR, XPS and elemental analysis all indicated that ultrafine MnOx particles were attached to the biochar surface. The surface properties and composition of the oxygen-containing functional groups were enhanced by $KMnO_4$ modification. Batch sorption experiments showed that MnOx-SBC's TC-adsorption capacity was 105.9 $mg{\cdot}g^{-1}$, 46.4% higher than SBC's. The TC-adsorption onto MnOx-SBC agreed well with the pseudo-second-order model and Freundlich isotherm. A new platform is proposed for reusing swine manure while solving the livestock industry's antibiotic pollution risk by 'treating waste with waste'.

Key words: adsorption, biochar, modification, swine manure, tetracycline

HIGHLIGHTS

- TC adsorption capacity of swine manure derived biochar enhanced after $KMnO_4$ modification.
- Initial solution pH, temperature and initial solution concentration affected TC removal.
- Pseudo-second-order and Freundlich models can well fit the adsorption behavior.
- Adsorption mechanism included pore-filling, surface complexation, π-π interactions and H-bonding.

GRAPHICAL ABSTRACT

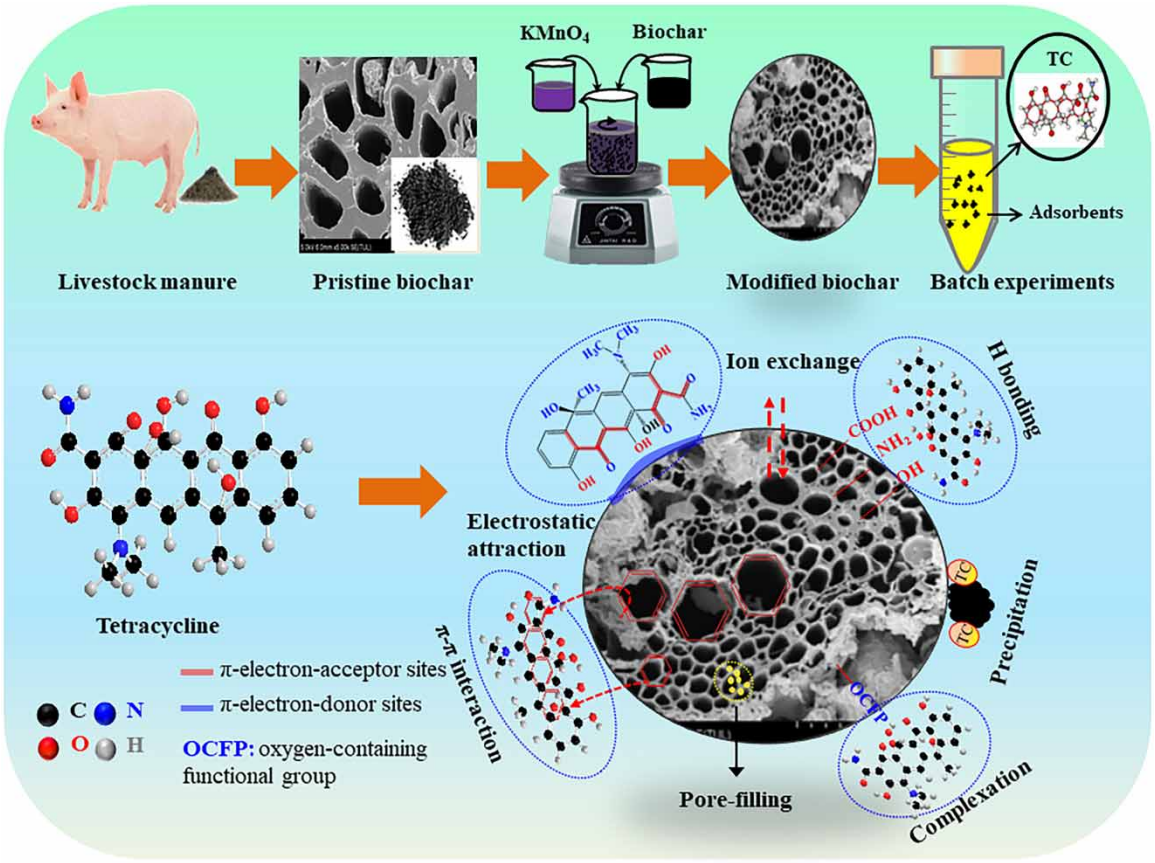

1. INTRODUCTION

Antibiotics are used widely in animal and human medicine to prevent or treat infectious diseases (Marzbali *et al.* 2016). Over 25,000 tons of antibiotics are used annually in China, approximately 32% of which are applied as feed additives (Dai *et al.* 2019). Tetracycline (TC) is the most commonly used antibiotic, is produced at large-scale and widely available in the market. However, more than 70% of TC cannot be digested directly by animals, the undigested TC being excreted and it accumulates in the soil, sediment and aquatic environments (Luo *et al.* 2011; Guo *et al.* 2022). Livestock wastes are a major source of undigested TCs and antibiotic resistance genes in the environment (Zhou *et al.* 2017). Worse still, currently available livestock waste treatment processes, such as composting, do not mitigate their dissemination efficiently into the environment and they may even be enriched after composting (Berendonk *et al.* 2015). Therefore, there is an urgent need to find a sustainable and practical method of removing residual TC from livestock industry wastewater.

Considering its simplicity and high removal efficiency, adsorption was considered as a good practical choice for TC removal (Chen *et al.* 2017a; Liang *et al.* 2018). Biochar is a porous, stable and carbon-rich solid, produced by the pyrolysis of agricultural wastes, animal manure, sewage sludge and other organic wastes, in an oxygen-limited environment (Chen *et al.* 2017b; Leng *et al.* 2021). It has been used widely as the adsorbent for pollutant removal due to its high specific surface, heterogeneous pore structure, and large surface functional groups, but its efficiency varies considerably for different feedstocks, pyrolysis conditions, modifying agents and other factors (Cole *et al.* 2017). The preparation of livestock waste-derived biochar could limit the negative environmental effect efficiently by reducing the CO_2 emitted and treating wastewaters released by the livestock industry, which is often contaminated with TC (Li *et al.* 2017a; Wang *et al.* 2018). In addition, in preparing biochar, the antibiotic residues and pathogens in livestock waste would be eliminated, reducing the risk of these hazardous materials entering the environment. However, although much attention has been placed on livestock waste-derived biochar's apparent ability to remove pollutants (Mitchell *et al.* 2015), its adsorption capacities

vary remarkably. For example, the TC adsorption capacities of some biochars exceeds 1536 mg g^{-1} (Yang *et al.* 2019), but that of most biochar for TC is below 50 mg g^{-1} (Luo *et al.* 2019; Tan *et al.* 2019).

Various methods have been adopted to alter the specific surface, functional groups, porous structures or other physicochemical characteristics of pristine biochar, to improve its adsorption performance (Vithanage *et al.* 2016). $KMnO_4$ is considered an effective adsorbents modification reagent, with great potential to accelerate the adsorption rate and enhance the pollutant removal performance of biochar (Cantu *et al.* 2014; Song *et al.* 2014; Zhang *et al.* 2020). $KMnO_4$ acts not only as a potent oxidizing agent but also as the precursor of MnO_x, thus forming novel, engineered biochars. Previous studies have found that $KMnO_4$ modification improves the number of oxygen-containing functional groups (OCFPs), enlarges the specific surface, and provides more active sites on biochar (Feng *et al.* 2014). However, biochar derived from animal manure usually has high ash content, with a relatively higher oxygen/carbon ratio and lower specific surface (Zhao *et al.* 2016). Thus, the TC removal performance may differ from other biochars. 'Treating waste with waste', using animal manure-derived biochar as a scavenger for wastewater may therefore be a promising and practical measure.

In this study, swine manure was chosen as the biochar feedstock and $KMnO_4$ as the activator to further improve its sorption capacity. The study's aim's were to: (1) compare the properties of animal manure-derived biochar before and after $KMnO_4$ modification; (2) evaluate the TC sorption capacity of MnO_x-SBC; and (3) clarify the possible mechanisms of TC adsorption on livestock waste derived biochar.

2. MATERIALS AND METHODS

2.1. Materials

Swine manure was collected from a pig farm in Liaocheng, China. TC ($C_{22}H_{24}N_2O_8$, purity >98.5%) was purchased from Macklin Co., Ltd. (Shanghai, China). All other chemicals used, including HCl, NaOH, and $KMnO_4$, were analytical grade and obtained from Sinopharm Company, China.

2.2. Biochar preparation

Air-dried swine manure was ground to pass through a 2 mm sieve, packed into a ceramic pot and pyrolyzed at 450 °C for 4 hours in a tube furnace (heating rate 15 °C min^{-1} and N_2 flow rate 50 mL min^{-1}). The resulting biochar, marked as SBC, was washed, dried at 60 °C to a constant weight and sieved for the 0.15–0.45 mm fraction for analysis.

The biochar adaptation with $KMnO_4$ was conducted as described in the literature with some modifications (Chen *et al.* 2018): 5.0 g SBC was immersed in 500 mL 5% $KMnO_4$ solution and concussed ultrasonically for 24 hours, then heated at 450 °C for 1 hour in a muffle furnace and washed with distilled water. The biochar was then dried at 105 °C for 24 hours, and marked as MnO_x-SBC for characterization and batch experiments.

2.3. Characterization

A scanning electron microscope (SEM, SU8010, Japan) equipped with an energy-dispersive X-ray spectroscope (EDS, Horiba EX-350, Japan) was used to determine the biochar's morphology and the main elements on its surface. Surface functional groups were identified by Fourier transform infrared spectroscopy (FTIR, Nicolet 6700, Thermo Electron Scientific Inc., USA). The specific surface, porosity and pore volume were determined by Brunauer-Emmett-Teller analysis (BET, ASAP2020, USA). The XPS spectra were obtained on an Escalab250Xi (Thermo Fisher Technologies, Escalab 250XI, USA). The point of zero charge (pH_{pzc}) was estimated by the pH drift method (Jang *et al.* 2018).

2.4. Batch experiments

Initial solution pH effects on TC removal performance were investigated using batch experiments with the pH ranging from 2 to 11. The initial pH was adjusted using 0.1 mol L^{-1} HCl or NaOH solution. Approximately 10 mg of adsorbent (SBC and MnO_x-SBC, respectively) was added to brown glass tubes containing 40 mL TC solution (200 mg L^{-1}) at different pHs. The tubes were placed in an opaque shaker and shaken at 180 rpm for 24 hours. After filtration with a 0.22 μm syringe filter, the filtrate's residual TC concentration was measured by spectrophotometry at $\lambda = 365$ nm (Xiang *et al.* 2020). Blank experiments without biochar addition were also conducted to eliminate TC decomposition.

For the kinetic adsorption experiments, approximately 10 mg biochar was added to 80 mL TC solution (200 mg L^{-1}, pH unadjusted) in brown glass tubes, and shaken at 180 rpm for 24 hours. Samples were taken at regular intervals and measured at λ 365 nm.

For the adsorption isotherms, approximately 10 mg of biochar added to 40 mL TC solution at different initial concentrations (25–300 mg L^{-1}, pH unadjusted) and shaken for 24 h. The residual TC concentration in the filtrate was measured as above.

The effects of temperature on TC adsorption were determined in batch experiments at different initial TC concentrations (25–300 mg L^{-1}) and 25, 35, and 45 °C, respectively. Other procedures were as above.

3. RESULTS AND DISCUSSION

3.1. Biochar characterization

After $KMnO_4$ modification, the proportion of C in MnO_x-SBC had decreased and that of O increased (Table 1), which is attributed to the oxidizing effect of $KMnO_4$. The attachment of MnO_x particles also lowered the proportion of other elements. The ratios of O/C and (O + N)/C in MnO_x-SBC were also slightly higher than those of pristine biochar, which was consistent with results obtained by others (Liao *et al.* 2022). The lower H/C means higher aromaticity, while higher O/C indicates greater polarity (Dieguez-Alonso *et al.* 2019).

Table 1 | Elemental compositions and physio-chemical properties of SBC and MnO_x-SBC

				Elemental composition (%)				Atomic ratio		
Adsorbent	Specific surface ($m^2\ g^{-1}$)	Pore volume ($cm^3\ g^{-1}$)	Ash (%)	C	H	O[a]	N	H/C	O/C	(O + N)/C
SBC	41.58	0.08	46.50	44.10	1.01	7.30	0.84	0.02	0.17	0.18
MnO_x-SBC	66.27	0.13	49.04	39.85	1.18	9.05	0.79	0.03	0.23	0.25

[a]O (%) = 100%-C(%)-N(%)-H(%)-ash(%).

The surface of SBC was smooth and carried some pore structures (Figure 1). After $KMnO_4$ modification, MnO_x-SBC's porous structure was more apparent and had numerous particles attached to the pore edges, offering more active TC adsorption sites. Like the element analysis, the EDS data also indicate increased O content, possibly due to the increased oxygen-containing functional groups after $KMnO_4$ modification (Zhang *et al.* 2020). The appearance of Mn peaks in MnO_x-SBC also confirmed the attachment of Mn-containing compounds to the biochar. This is consistent with the results of the elemental analysis.

After $KMnO_4$ modification, the SBC's pore volume and BET surface changed from 0.082 $cm^3 \cdot g^{-1}$ and 41.58 $m^2 \cdot g^{-1}$ to 0.134 and 66.27, respectively (Table 1). The adsorbent's pores were divided by International Union of Pure and Applied Chemistry (IUPAC) into micro-, meso- and macro-pores, according to the pore diameter (Li *et al.* 2017b). With a sufficiently large biochar pore diameter, the large microporous structure allowed TC molecules to enter the pores quickly and become distributed evenly on its surface, leading to MnO_x-SBC's superior removal performance. Due to the size exclusion effect, the biochar pore diameter should be at least 1.7 times that of the TC molecule, indicating that the pore-filling participates in TC adsorption.

The MnO_x-SBC functional groups were analyzed by FTIR spectra before and after TC adsorption (Figure 2). The oxygen-containing functional groups, which acted as π-electron acceptors for biochar during TC adsorption, including –OH at 3424 cm^{-1}, –C = O on aromatic rings at 1735 cm^{-1}, and C–O–C at 1034.6 cm^{-1} changed to some extent compared with those of SBC. The Mn-O vibration at 547.1 cm^{-1} was observed in MnO_x-SBC, indicating the successful formation of Mn–O on the biochar surface. In addition, the C–H stretching vibration of CH_2 and CH_3 (near 2858 cm^{-1}) in MnO_x-SBC was weaker than in SBC, indicating that $KMnO_4$ modification altered the structure of the biochar's C–H, amide bonds and aromatic ring (–CONH–, C = C), ultimately affecting the π-π conjugation between the aromatic ring structures in biochar and in TC (Xu *et al.* 2022). The formation of hydrogen bonds between the biochar's oxygen-containing functional groups and the TC's phenolic group could also facilitate the TC adsorption process (Dai *et al.* 2019). After TC adsorption, some organic functional group peaks – e.g., Mn–O, –OH, C–O–C, and aromatic structures – were shifted, indicating that these active groups participated in TC removal. However, the composition of SBC's functional group did not change significantly after TC adsorption, probably because the main biochar functional groups were similar to TC.

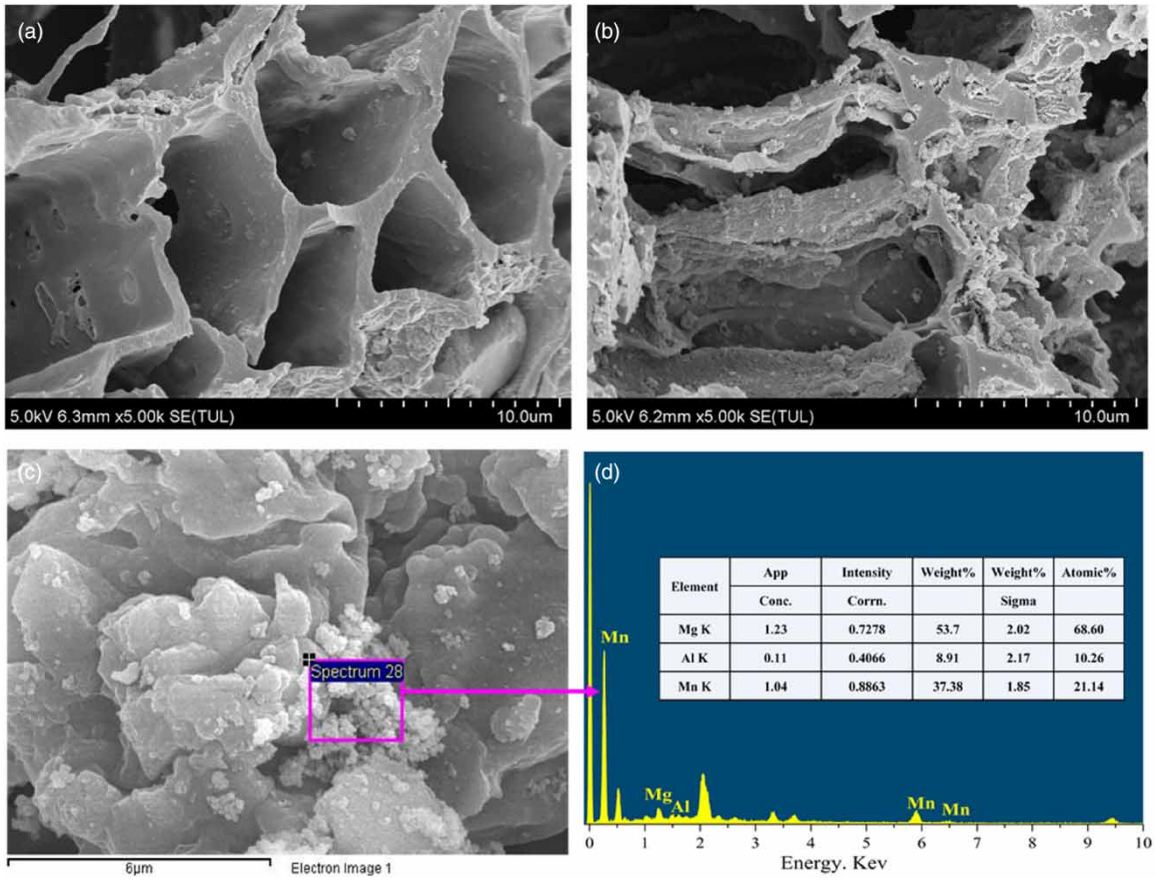

Figure 1 | SEM–EDS biochar scans. (a) SEM of swine manure-derived biochar; (b) SEM of swine manure-derived biochar after $KMnO_4$ modification; (c, d) site image and EDS of swine manure-derived biochar after $KMnO_4$ modification.

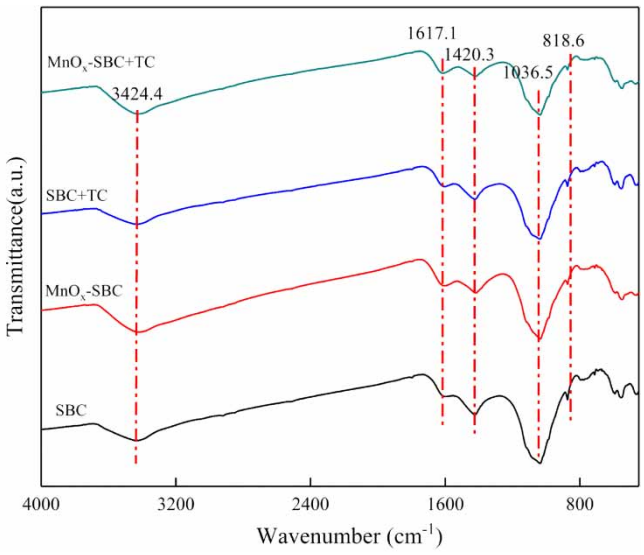

Figure 2 | FTIR spectra of swine manure-derived biochar before and after TC adsorption.

The MnO_x-SBC functional groups were also analyzed by XPS (Figure 3). Analysis of the Mn2p spectra revealed a firm Mn peak at 642.7 and 654.5 eV binding energy in MnO_x-SBC (Figure 3(d)), which further confirmed that MnO_x was introduced successfully into biochar during modification. The C1s spectra analysis of MnO_x-SBC (Figure 3(b)) revealed five peaks in the C1s. The peaks' binding energy values corresponding to C–F

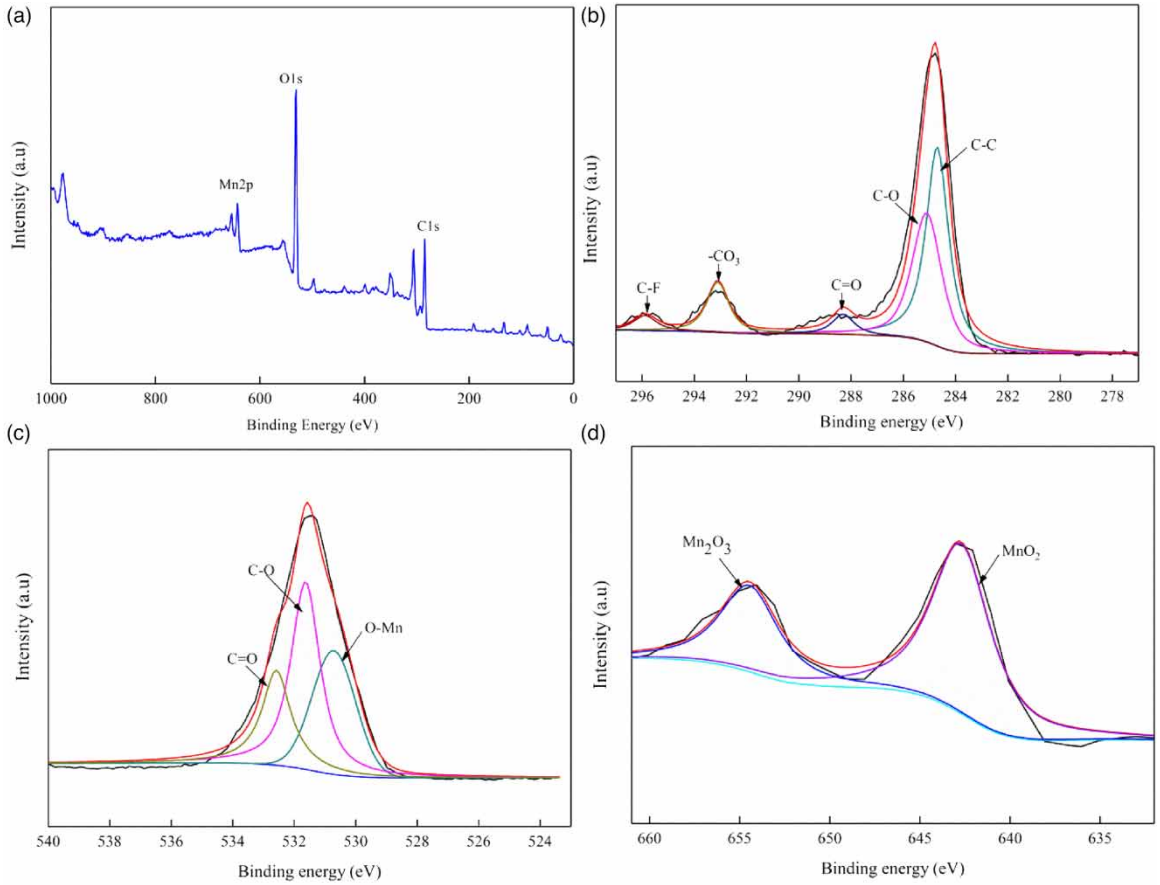

Figure 3 | XPS survey spectrum (a), C1s XPS scanning diagram (b), O1s XPS scanning diagram (c), and Mn2p XPS scanning diagram (d) of MnO_x-SBC.

(293.1 eV) and $-CO_3$ groups (295.9 eV), were seen as well as those of the components of carbon species in the form of C–O bonds (phenolic, alcohol, or ether groups) at 285.1–285.3 eV, and carbon double-bonded to O (C=O) bonds at 288.2–288.6 eV. For the O1s spectra of $KMnO_4$-modified biochar (Figure 3(c)), the binding energy values showed three main peaks, which corresponded to C=O bonds in ketone, carbonyl, or quinone groups at 531.6 eV (Guedidi *et al.* 2013); C–O bonds in R-OH and C–O–C groups at 532.6 eV (Ling *et al.* 2017) and the Mn–O groups. This all suggested that TC sorption would probably improve, since MnO_x particles and oxygen-containing functional groups have a strong bonding affinity to TC in aqueous solution (Xiang *et al.* 2020).

3.2. Effect of initial solution pH, concentration and temperature

Biochar's TC absorption capacity is affected significantly by changes in both initial TC concentration and pH (Chen *et al.* 2018). TC is hydrophilic and amphiphilic, with three pKa values 3.3, 7.7 and 9.7 (Figure 4(b)). The difference in biochar's pH_{PZC} and TC's pK_a were considered the dominant factors for the changes in biochar's TC removal performance at different pHs. TC exists mainly as a cation (TCH_3^+) in acid conditions, as a zwitterion (TCH_2^0) in near neutral or slightly acidic states, and as an anion (TCH^- and/or TC^{2-}) in an alkaline environment (Xu & Li 2010; Xu *et al.* 2022). In this study, TC adsorption performance was maximized at pH = 2 on MnO_x-SBC (104.2 $mg \cdot g^{-1}$), some 53% higher than pristine biochar. As the pH increased, TC removal performance decreased until the pH exceeded 4, above which level it remained stable (Figure 4(c)).

The predominant component of TC was TCH_2^0 when the initial solution pH was below 4.0, but became TCH^- and TC^{2-} when the pH exceeded 7.7 (Jang *et al.* 2018). Increasing the pH increased deprotonation of the functional groups on the biochar surface, so that the TC combined with the biochar by co-precipitation, ion exchange, and complexation (Zhang *et al.* 2020). This reduced the adsorption affinity of biochar for TC, and the adsorption capacity fell at high pH (Xu & Li 2010). However, large amounts of TC were still adsorbed by MnO_x-SBC, indicating that other effects, such as pore filling, π-π action and H bonding, also played essential roles (Wang *et al.*

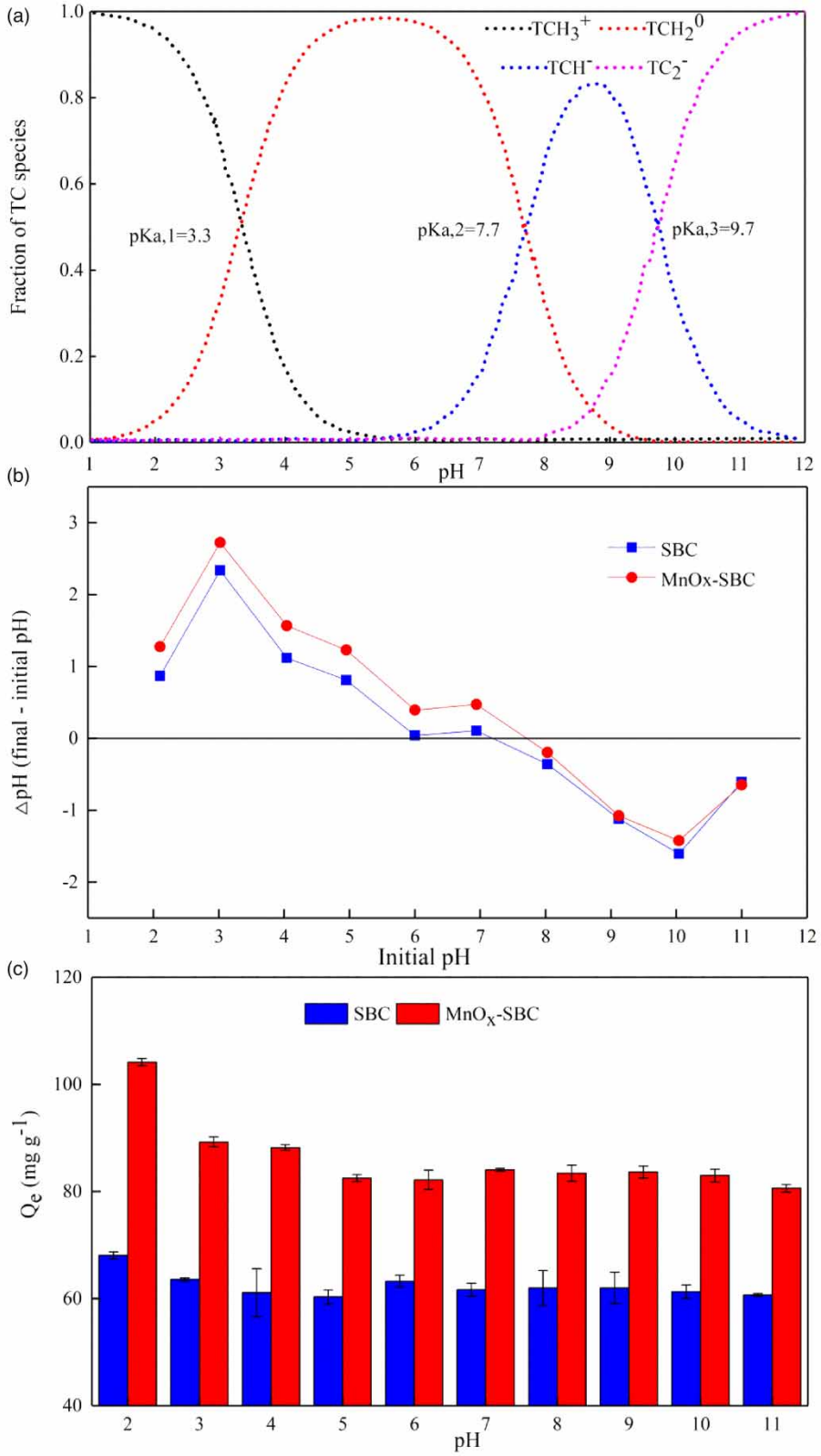

Figure 4 | TC speciation (a), pH_{PZC} values of different absorbents (b), and, influence of pH on biochar's TC adsorption capacity (c).

2020). In summary, MnO_x-SBC can adsorb sufficient TC across a range of pH values, with broad application prospects in TC removal.

The effect of initial solution concentration on biochar's TC adsorption capacity, before and after $KMnO_4$ modification, is shown in Figure 5. The TC adsorption capacity increased gradually with increasing initial

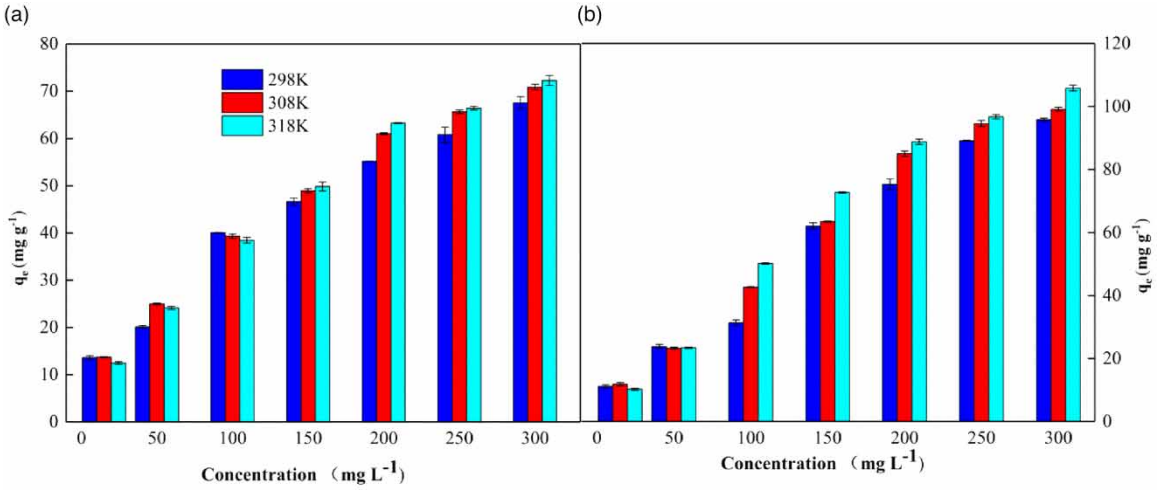

Figure 5 | Effect of initial solution concentration of TC on adsorption capacity at different temperature of SBC (a) and MnO_x-SBC (b).

concentration until the initial concentration was over 200 mg·L^{-1}, but remained almost unchanged above that. In the initial adsorption stage, TC molecules can transfer from aqueous solution to the biochar surface due to the abundance of unoccupied adsorption sites, large surface area, and high TC concentration (Marzbali *et al.* 2016). Once most adsorption sites were occupied by TC, the adsorption rate slowed when the TC concentration increased (Song *et al.* 2014).

With increasing temperature, the TC adsorption capacity of both pristine and $KMnO_4$-modified biochar also gradually increased (Figure 6). Higher temperatures accelerate TC intermolecular motion and promotes the diffusion rate to the biochar surface (Gao *et al.* 2012), thus facilitating the biochar's TC adsorption capacity. Thermodynamic analysis (Figure 6(b)) shows that TC adsorption on MnO_x-SBC is spontaneous and endothermic, with $\Delta G < 0$ and $\Delta H > 0$. Furthermore, $\Delta S > 0$ also suggested that TC adsorption on biochar is irreversible. Proportional TC removal increased with temperature, indicating that biochar's TC adsorption capacity is affected significantly by temperature (Gao *et al.* 2012). Nevertheless, higher temperatures promote adsorption, with a relatively higher biochar TC adsorption capacity than at room temperature, on which basis 25 °C was selected as the optimum temperature for convenient operation.

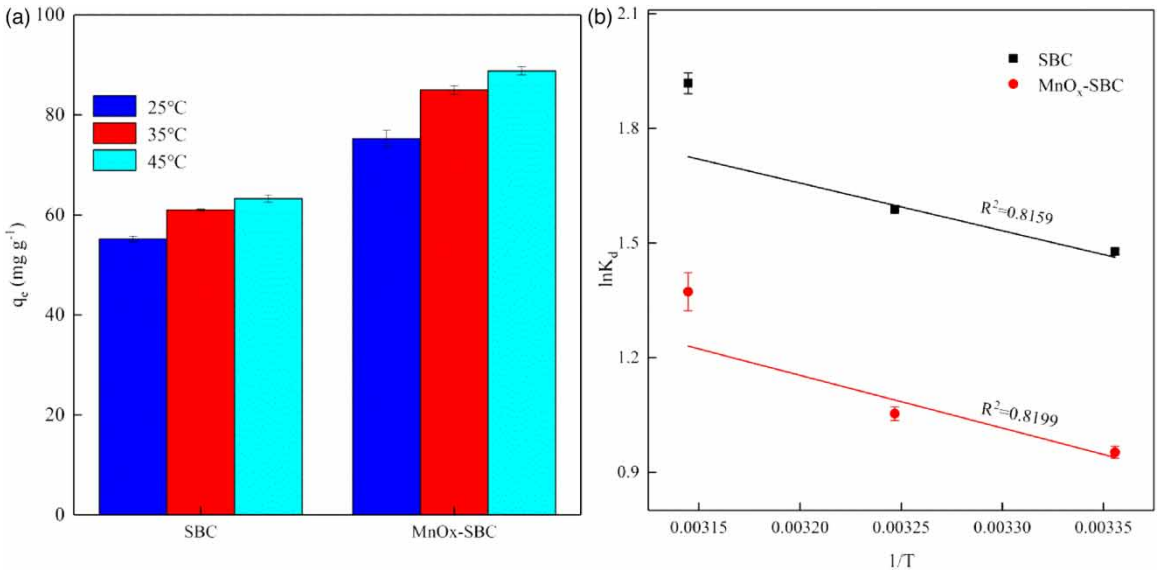

Figure 6 | Effect of temperature on biochar's TC adsorption at 25, 35 and 45 °C (a), and, thermodynamic model (b).

3.3. Adsorption kinetics

As shown in Figure 7, a fast TC adsorption phase was followed by a slow one for both the pristine and modified biochar. The capacity of MnO_x-SBC reached the adsorption balance after about 120 minutes, indicating quick TC adsorption by $KMnO_4$-modified biochar. TC molecules can transfer easily from aqueous solution to the adsorbent surface in the initial stage because of the large specific surface, with abundant active adsorption sites and a high TC solution concentration (Chen *et al.* 2017a). When most adsorption sites were combined with TC, the adsorption rate slowed because fewer sites remained (Dai *et al.* 2019). Although the highest biochar TC adsorption capacity in our study was not as high as that of rice straw (Chen *et al.* 2018), eucalyptus sawdust (Wan *et al.* 2016), or camphor leaves (Hu *et al.* 2021), the maximum sorption capacities of MnO_x-SBC are similar to or exceed those of these adsorbents, indicating that livestock-derived biochar has great potential for TC removal.

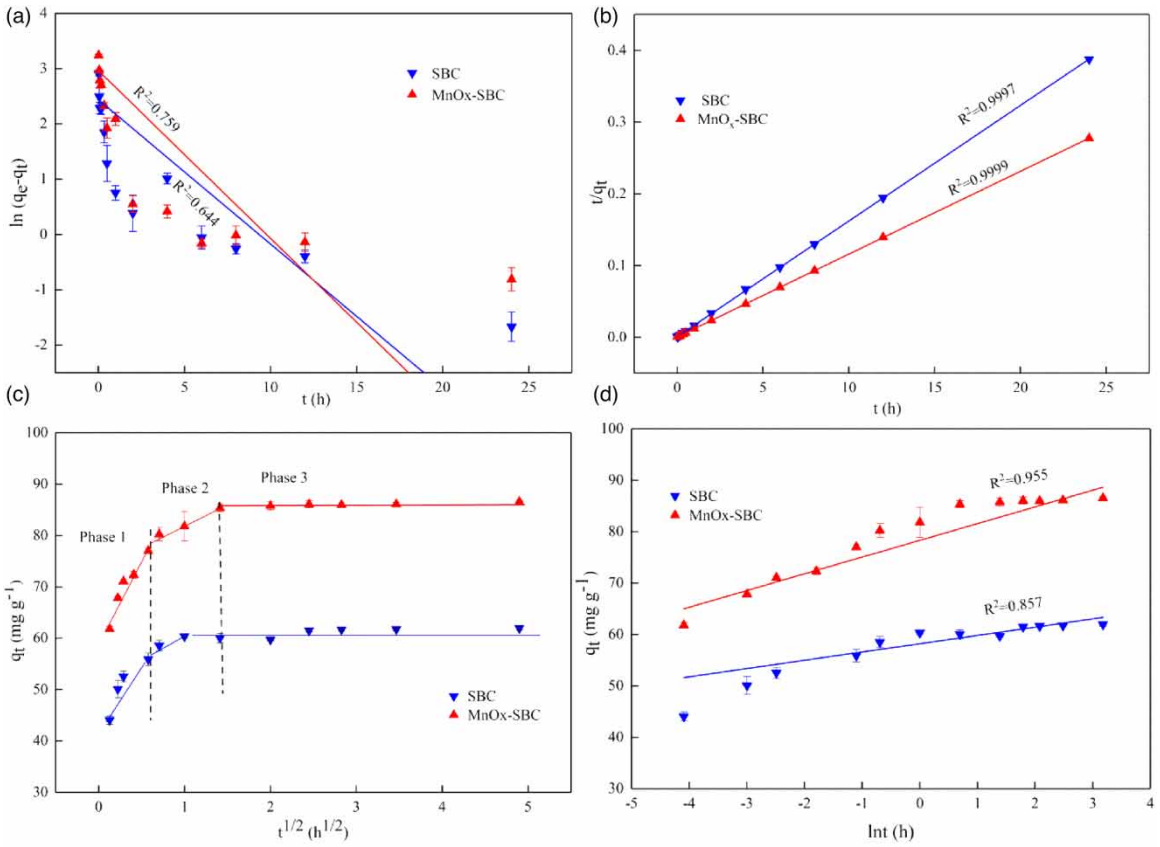

Figure 7 | Kinetics spectra for TC sorption on different biochars (a), PFO plots; (b) PSO plots (c); intraparticle diffusion model; and (d) Elovich model. Dosage, 0.2 g; temperature, 25 °C; initial concentration, 200 mg L^{-1}; initial pH, unadjusted.

Kinetic models, including the pseudo-first-order (PFO), pseudo-second-order (PSO), interparticle diffusion and Elovich models, were applied to estimate the biochar TC adsorption rate and determine the adsorption equilibrium time (Table 2). The PSO model's R^2 for MnO_x-SBC was higher than that of the PFO and Elovich models, which is consistent with previous results (Du *et al.* 2021). According to the PSO model, biochar's TC

Table 2 | **TC** adsorption kinetics parameters onto SBC and MnO_x-SBC

	PFO			PSO		
Parameters	**q_e (mg g^{-1})**	**K_1 (h^{-1})**	**R^2**	**q_e (mg g^{-1})**	**K_2 (g mg^{-1} h^{-1})**	**R^2**
SBC	62.69	0.261	0.779	62.01	0.396	0.9997
MnO_x-SBC	87.09	0.303	0.674	86.58	0.336	0.9999

adsorption has two dynamic steps: a single layer of TC molecules forming first, with TC molecules adsorbed on the biochar's micropore surface, with chemisorption then becoming the dominant process as monolayer physical adsorption approaches saturation (Jing *et al.* 2014). The TC reaction process on MnO_x-SBC is also rapid because the adsorption rate constant K is less than 1, indicating that TC adsorption on MnO_x-SBC comprises chemisorption and physical capture (Hu *et al.* 2021).

The intraparticle and liquid film diffusion process results indicate that intraparticle diffusion was involved, and occurred mainly on the surface (Figure 6(c)). However, the large fitting curve intercept for both MnO_x-SBC and SBC suggests that the intraparticle diffusion process was a major speed-limiting step but not the only one – boundary layer diffusion or external mass transfer may also have been involved.

3.4. Adsorption isotherms

The Langmuir and Freundlich isotherm models were used to analyze the relationship between the equilibrium concentration of TC in solution and MnO_x-SBC's equilibrium adsorption capacity for TC (Figure 8 and Table 3). According to the Langmuir model, adsorption occurs on homogeneous surfaces with uniform adsorbent sites (Norvill *et al.* 2017), but on heterogeneous surface and unequal binding sites in the Freundlich model (Taheran *et al.* 2016). The MnOx-SBC results fitted better with the Freundlich than the Langmuir isotherm model (Table 3).

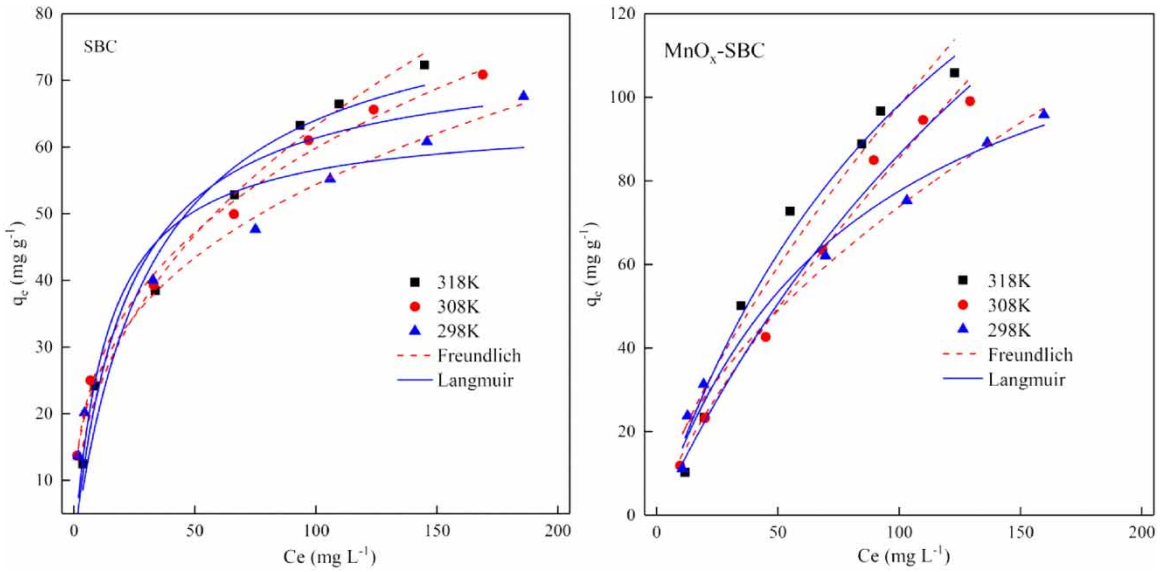

Figure 8 | Adsorption isotherms: SBC Langmuir and Freundlich models (a) and MnO_x-SBC (b) at different temperatures.

Table 3 | TC adsorption isotherm parameters on SBC, MnO_x-SBC, DBC, and MnO_x-DBC

	Temperature (K)	298			308			318		
Model	Sample	q_{max} (mg g^{-1})	K_L (L mg^{-1})	R^2	q_{max} (mg g^{-1})	K_L (L mg^{-1})	R^2	q_{max} (mg g^{-1})	K_L (L mg^{-1})	R^2
Langmuir	SBC	67.57	0.056	0.918	70.88	0.058	0.917	72.29	0.053	0.942
	MnO_x-SBC	95.81	0.031	0.911	99.11	0.029	0.805	105.85	0.033	0.805
		K_f ($mg^{(1-n)}$ L^n g^{-1})	n	R^2	K_f ($mg^{(1-n)}$ L^n g^{-1})	n	R^2	K_f ($mg^{(1-n)}$ L^n g^{-1})	n	R^2
Freundlich	SBC	12.192	3.080	0.994	12.341	2.9168	0.994	8.688	2.321	0.992
	MnO_x-SBC	4.817	1.687	0.983	2.271	1.269	0.984	3.516	1.384	0.950

The maximum TC adsorption capacity of MnO_x-SBC reached 95.81, 99.11 and 105.85 mg g^{-1}, respectively, at 298, 308 and 318 K (Table 3), 39.8–46.4% higher than those of SBC. MnO_x-SBC's enhanced TC adsorption capacity may be attributable to its abundant OCFPs, larger specific surface and higher oxygen/carbon ratio.

The values of R_L and n^{-1} were 0.923 and 0.021, respectively, suggesting a high affinity and numerous suitable adsorption sites on MnO_x-SBC for TC species (Huang *et al.* 2018).

3.5. Adsorption mechanisms

According to the analysis above, the TC adsorption mechanism on MnO_x-SBC comprises mainly pore-filling, π–π electron donor-acceptor (EDA) interaction, electrostatic interaction, H-bonding, and surface complexation with oxygen-containing functional groups (Figure 9). SEM and BET analysis showed that, after $KMnO_4$ modification, some SBC micropores disappeared, while the proportion of mesopores increased, implying that pore-filling mechanisms (microporous retention) play an essential role in TC adsorption by biochar.

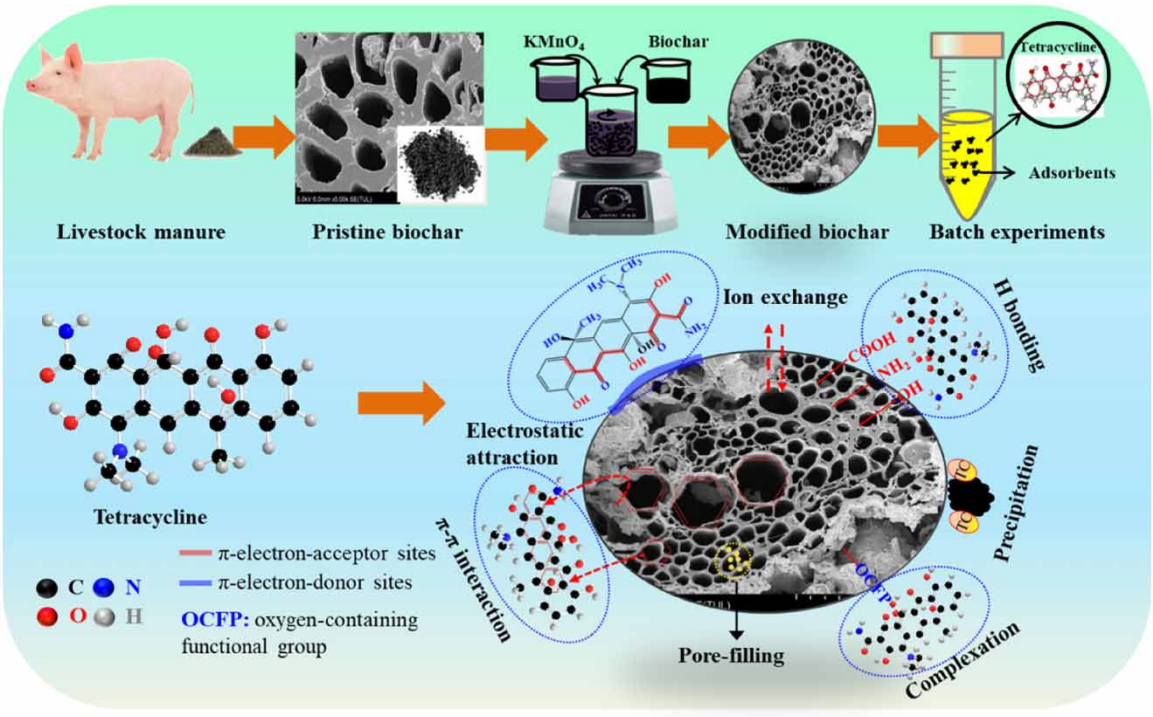

Figure 9 | Schematic diagram of TC adsorption mechanism on MnO_x-SBC.

Generally, the π-π EDA interaction was weak at low pH, since TC molecules are cationic and the biochar surface is commonly positive (Mitchell *et al.* 2015). With increasing pH, TC becomes zwitterionic, and the EDA interaction between TC and biochar is strengthened (Yang *et al.* 2019). However, MnO_x-SBC's TC removal performance is relatively high with pH between 4 and 11 in this study, indicating that electrostatic interaction participated in TC adsorption but was not the dominant factor.

FTIR analysis showed that, after TC adsorption, the position of the stretching peak of each functional group – C–O–C in the aromatic ring structure, and C=O and O–H in the alcohol and phenol – had shifted. It was concluded that the aromatic group participated in the entire adsorption process (Chen *et al.* 2018), and π-π conjugation formed between aromatic structures, including C–O–C and C=O in the biochar and the aromatic ring structure in TC. The H-bonding between -OH and the oxygen-containing functional groups also facilitated adsorption (Zhang *et al.* 2020). In summary, the difference in the adsorption mechanisms could be responsible for the changes in the interactions of TC absorbed by MnO_x-SBC.

4. CONCLUSIONS

$KMnO_4$ modification alters the surface structures and properties of SBC, further enhancing the TC removal performance of MnO_x-SBC. MnO_x-SBC's TC adsorption behavior was a spontaneous, endothermic, and monolayer chemical process. The process is best fitted by the pseudo-second-order model and Freundlich model. TC adsorption onto the MnO_x-SBC surface is caused mainly by electrostatic interaction, pore-filling, π-π conjugation, H-bonding and complexation of the oxygen-containing functional groups. Biochar derived from

swine manure, especially after $KMnO_4$ modification, may thus be suitable for removing TC from aqueous solution by sorption.

ACKNOWLEDGEMENTS

This study was supported by the Natural Science Foundation of China (Grant No. 41807092), The Open Project of Liaocheng University Animal Husbandry Discipline (No. 319312101-18), the Project of Shandong Province Higher Educational Science and Technology Program (KJ2018BAF034), and the Startup Foundation for Ph.D. of Liaocheng University (318051839).

CONTRIBUTION STATEMENT

Zan Fu: Conceptualization, resources, writing original draft. Yurong Chen: Investigation, data curation. Yanyan Lu: Methodology, formal analysis. Yue Wang: Investigation, data curation. Jiahui Chen: Methodology, formal analysis. Youxin Zhao: Writing, review and editing. Xiaofei Tian: Supervision, writing review and editing, and funding acquisition.

DATA AVAILABILITY STATEMENT

Data cannot be made publicly available; readers should contact the corresponding author for details.

CONFLICT OF INTEREST

The authors declare there is no conflict.

REFERENCES

Berendonk, T. U., Manaia, C. M., Merlin, C., Fatta Kassinos, D., Cytryn, E., Walsh, F., Bürgmann, H., Sørum, H., Norström, M. & Pons, M. N. 2015 Tackling antibiotic resistance: the environmental framework. *Nat. Rev. Microbiol.* **13**, 310–317.

Cantu, Y., Remes, A., Reyna, A., Martinez, D., Villarreal, J., Ramos, H., Trevino, S., Tamez, C., Martinez, A., Eubanks, T. & Parsons, J. G. 2014 Thermodynamics, kinetics, and activation energy studies of the sorption of chromium (III) and chromium (VI) to a Mn_3O_4 nanomaterial. *Chem. Eng. J.* **254**, 374–383.

Chen, J., Liu, Y. S., Zhang, J. N., Yang, Y. Q., Hu, L. X., Yang, Y. Y., Zhao, J. L., Chen, F. R. & Ying, G. G. 2017a Removal of antibiotics from piggery wastewater by biological aerated filter system: treatment efficiency and biodegradation kinetics. *Bioresour. Technol.* **238**, 70–77.

Chen, W., Yang, H., Chen, Y., Xia, M., Chen, X. U. & Chen, H. 2017b Transformation of nitrogen and evolution of n-containing species during algae pyrolysis. *Environ. Sci. Technol.* **51**(11), 6570–6579.

Chen, T. Y., Luo, L., Deng, S. H., Shi, G. Z., Zhang, S. R., Zhang, Y. Z., Deng, O. P., Wang, L. L., Zhang, J. & Wei, L. Y. 2018 Sorption of tetracycline on H_3PO_4 modified biochar derived from rice straw and swine manure. *Bioresour. Technol.* **267**, 431–437.

Cole, A. J., Paul, N. A., de Nys, R. & Roberts, D. A. 2017 Good for sewage treatment and good for agriculture: algal based compost and biochar. *J. Environ. Manage.* **200**, 105–113.

Dai, Y. J., Zhang, K. X., Li, J. J., Meng, X. B., Guan, X. T., Sun, Q. Y., Sun, Y., Wang, W. S., Lin, M., Liu, M., Yang, S. S., Chen, Y. J., Gao, F., Zhang, X. & Liu, Z. H. 2019 New use for spent coffee ground as an adsorbent for tetracycline removal in water. *Chemosphere* **215**, 163–172.

Dieguez-Alonso, A., Anca-Couce, A. & Frišták, V. 2019 Designing biochar properties through the blending of biomass feedstock with metals: impact on oxyanions adsorption behavior. *Chemosphere* **214**, 743–753.

Du, C., Zhang, Z., Yu, G., Wu, H., Chen, H., Zhou, L., Zhang, Y., Su, Y., Tan, S., Yang, L., Song, J. & Wang, S. 2021 A review of metal organic framework (MOFs)-based materials for antibiotics removal via adsorption and photocatalysis. *Chemosphere* **272**, 129501.

Feng, L. L., Xuan, Z. W., Zhao, H. B., Bai, Y., Guo, J. M., Su, C. W. & Chen, X. K. 2014 Mno_2 prepared by hydrothermal method and electrochemical performance as anode for lithium-ion battery. *Nanoscale Res. Lett.* **9**, 290–297.

Gao, Y., Li, Y., Zhang, L., Huang, H., Hu, J. J., Shah, S. M. & Su, X. G. 2012 Adsorption and removal of tetracycline antibiotics from aqueous solution by graphene oxide. *J. Colloid Interface Sci.* **368**, 540–546.

Guedidi, H., Reinert, L., Lévêque, J. M., Soneda, Y., Bellakhal, N. & Duclaux, L. 2013 The effects of the surface oxidation of activated carbon, the solution pH and the temperature on adsorption of ibuprofen. *Carbon* **54**, 432–443.

Guo, X., Peng, Y., Li, N., Tian, Y., Dai, L., Wu, Y. & Huang, Y. 2022 Effect of biochar-derived DOM on the interaction between Cu(II) and biochar prepared at different pyrolysis temperatures. *J. Hazard. Mater.* **421**, 126739.

Hu, Y., Chen, D., Zhang, R., Ding, Y., Ren, Z., Fu, M., Cao, X. & Zeng, G. 2021 Singlet oxygen-dominated activation of peroxymonosulfate by passion fruit shell derived biochar for catalytic degradation of tetracycline through a non-radical oxidation pathway. *J. Hazard Mater.* **419**, 126495.

Huang, H., Yao, W. L., Li, R. H., Ali, A., Du, J., Guo, D., Xiao, R., Guo, Z. Y., Zhang, Z. Q. & Awasthi, M. K. 2018 Effect of pyrolysis temperature on chemical form, behavior and environmental risk of Zn, Pb and Cd in biochar produced from phytoremediation residue. *Bioresour. Technol.* **249**, 487–493.

Jang, H. M., Yoo, S. H., Choi, Y. K., Park, S. K. & Kan, E. S. 2018 Adsorption isotherm, kinetic modeling and mechanism of tetracycline on Pinus taeda-derived activated biochar. *Bioresour. Technol.* **259**, 24–31.

Jing, X. R., Wang, Y. Y., Liu, W. J., Wang, Y. K. & Jiang, H. 2014 Enhanced adsorption performance of tetracycline in aqueous solutions by methanol-modified biochar. *Chem. Eng. J.* **248**, 168–174.

Leng, L., Xiong, Q., Yang, L., Li, H., Zhou, Y., Zhang, W., Jiang, S., Li, H. & Huang, H. 2021 An overview on engineering the surface area and porosity of biochar. *Sci. Total Environ.* **763**, 144204.

Li, H. B., Dong, X. L., da Silva, E. B., de Oliveir, L. M., Chen, Y. S. & Ma, L. Q. 2017a Mechanisms of metal sorption by biochars: biochar characteristics and modifications. *Chemosphere* **178**, 466–478.

Li, M., Zhao, Z., Wu, X., Zhou, W. & Zhu, L. 2017b Impact of mineral components in cow manure biochars on the adsorption and competitive adsorption of oxytetracycline and carbaryl. *RSC Adv.* **7**(4), 2127–2136.

Liang, S., Lin, H., Yan, X. & Huang, Q. 2018 Electro-oxidation of tetracycline by a Magnéli phase Ti_4O_7 porous anode: kinetics, products, and toxicity. *Chem. Eng. J.* **332**, 628–636.

Liao, J., Ding, L., Zhang, Y. & Zhu, W. K. 2022 Efficient removal of uranium from wastewater using pig manure biochar: understanding adsorption and binding mechanisms. *J. Hazard Mater.* **423**, 127190.

Ling, L. L., Liu, W. J., Zhang, S. & Jiang, H. 2017 Magnesium oxide embedded nitrogen self-doped biochar composites: fast and high-efficiency adsorption of heavy metals in an aqueous solution. *Environ. Sci. Technol.* **51**, 10081–10089.

Luo, Y., Xu, L., Rysz, M., Wang, Y., Zhang, H. & Alvarez, P. J. J. 2011 Occurrence and transport of tetracycline, sulfonamide, quinolone, and macrolide antibiotics in the Haihe River Basin, China. *Environ. Sci. Technol.* **45**, 1827–1833.

Luo, J. P., Fang, R., Si, J. J., Zhang, X. Y., Tan, Z. Z. & Meng, Y. Y. 2019 Adsorption performance of tetracycline on nitric acid-modified rape biochar. *Environ. Technol.* **32**(2), 17–23. (In Chinese).

Marzbali, M. H., Esmaieli, M., Abolghasemi, H. & Marzbali, M. H. 2016 Tetracycline adsorption by H_3PO_4-activated carbon produced from apricot nut shells: a batch study. *Process Saf. Environ.* **102**, 700–709.

Mitchell, S. M., Subbiah, M., Ullman, J. L. & Frear, F. D. R. 2015 Call, evaluation of 27 different biochars for potential sequestration of antibiotic residues in food animal production environments. *J. Environ. Chem. Eng.* **3**, 162–169.

Norvill, Z. N., Toledo-Cervantes, A., Blanco, S., Shilton, A., Guieysse, B. & Munoz, R. 2017 Photodegradation and sorption govern tetracycline removal during wastewater treatment in algal ponds. *Bioresour. Technol.* **232**, 35–43.

Song, Z. G., Lian, F., Yu, Z. H., Zhu, L. Y., Xing, B. S. & Qiu, W. W. 2014 Synthesis and characterization of a novel MnO_x-loaded biochar and its adsorption properties for Cu^{2+} in aqueous solution. *Chem. Eng. J.* **242**, 36–42.

Taheran, M., Naghdi, M., Brar, S., Knystautas, E., Verma, M., Ramirez, A., Surampalli, R. & Valero, J. 2016 Adsorption study of environmentally relevant concentrations of chlortetracycline on pinewood biochar. *Sci. Total Environ.* **571**, 772–777.

Tan, Z., Zhang, X., Wang, L., Gao, B., Luo, J., Fang, R., Zou, W. & Meng, N. 2019 Sorption of tetracycline on H_2O_2-modified biochar derived from rape stalk. *Environ. Pollut. Bioavailab.* **31**, 198–207.

Vithanage, M., Mayakaduwa, S., Herath, I., Ok, Y. S. & Mohan, D. 2016 Kinetics, thermodynamics and mechanistic studies of carbofuran removal using biochars from tea waste and rice husks. *Chemosphere* **150**, 781–789.

Wan, S., Hua, Z., Sun, L., Bai, X. & Liang, L. 2016 Biosorption of nitroimidazole antibiotics onto chemically modified porous biochar prepared by experimental design: kinetics, thermodynamics, and equilibrium analysis. *Proc. Saf. Environ. Prot.* **104**, 422–435.

Wang, H., Fang, C., Wang, Q., Chu, Y., Song, Y., Chen, Y. & Xue, X. 2018 Sorption of tetracycline on biochar derived from rice straw and swine manure. *RSC Adv.* **8**(29), 16260–16268.

Wang, R. Z., Huang, D. L., Liu, Y. G., Zhang, C., Lai, C., Wang, X., Zeng, G. M., Zhang, Q., Gong, X. M. & Xu, P. 2020 Synergistic removal of copper and tetracycline from aqueous solution by steam-activated bamboo-derived biochar. *J. Hazard. Mater.* **384**, 121470.

Xiang, W., Wan, Y. S., Zhang, X. Y., Tan, Z. Z., Xia, T. T., Zheng, Y. L. & Gao, B. 2020 Adsorption of tetracycline hydrochloride onto ball-milled biochar: governing factors and mechanisms. *Chemosphere* **255**, 127057.

Xu, X. R. & Li, X. Y. 2010 Sorption and desorption of antibiotic tetracycline on marine sediments. *Chemosphere* **78**(4), 430–436.

Xu, J., Zhang, Y., Li, B., Fan, S. S., Xu, H. C. & Guan, D. X. 2022 Improved adsorption properties of tetracycline on KOH/$KMnO_4$ modified biochar derived from wheat straw. *Chemosphere* **296**, 133981.

Yang, J., Dai, J. D. & Wang, L. L. 2019 Ultrahigh adsorption of tetracycline on willow branche-derived porous carbons with tunable pore structure: isotherm, kinetics, thermodynamic and new mechanism study. *J. Taiwan Inst. Chem. E.* **96**, 473–482.

Zhang, J., Ma, X., Yuan, L. & Zhou, D. 2020 Comparison of adsorption behavior studies of Cd^{2+} by vermicompost biochar and $KMnO_4$-modified vermicompost biochar. *J. Environ. Manage.* **256**, 109959.

Zhao, B., Xu, R., Ma, F., Li, Y. & Wang, L. 2016 Effects of biochars derived from chicken manure and rape straw on speciation and phytoavailability of Cd to maize in artificially contaminated loess soil. *J. Environ. Manage.* **184**(Pt 3), 569–574.

Zhou, Y., Liu, X., Xiang, Y., Wang, P., Zhang, J., Zhang, F., Wei, J., Luo, L., Lei, M. & Tang, L. 2017 Modification of biochar derived from sawdust and its application in removal of tetracycline and copper from aqueous solution: adsorption mechanism and modelling. *Bioresour. Technol.* **245**(Pt A), 266–273.

First received 6 September 2022; accepted in revised form 13 October 2022. Available online 20 October 2022